

Article

A Solar Thermal Steam Propulsion System Using Disassociated Steam for Interplanetary Exploration

Leonard Vance ^{1,*}, Agustin Espinoza ¹, Jorge Martinez Dominguez ¹, Salil Rabade ², Gavin Liu ² and Jekan Thangavelautham ^{1,*}

¹ Aerospace and Mechanical Engineering Department, University of Arizona, Tucson, AZ 85721, USA

² School of Energy, Matter and Transport Engineering, Arizona State University, Tempe, AZ 85281, USA

* Correspondence: ldvance@email.arizona.edu (L.V.); jekan@arizona.edu (J.T.)

Abstract: Sustainable space exploration will require using off-world resources for propellant generation. Using off-world-generated propellants significantly increases future missions' range and payload capacity. Near Earth Objects (NEOs) contain a range of available resources, most notably water-ice and hydrated minerals. However, water-bearing regolith needs to be excavated and the water extracted. Water is a compelling choice for fuel as it is readily available in interplanetary space and easily stored. In this paper, we propose using solar concentrators, which can efficiently convert incident sunlight into heat without the need for moving parts. When water is heated up to 4000 K, a value consistent with high-performance refractive materials, it experiences significant disassociation into H₂, O₂, OH, H, and O components, providing a path for adding considerable additional chemical energy per degree of temperature increase, and producing theoretical specific impulse (I_{sp}) values in the range of 643 s to 659 s.

Keywords: small spacecraft; ISRU; steam disassociation; propulsion; system design



Citation: Vance, L.; Espinoza, A.; Martinez Dominguez, J.; Rabade, S.; Liu, G.; Thangavelautham, J. A Solar Thermal Steam Propulsion System Using Disassociated Steam for Interplanetary Exploration. *Aerospace* **2024**, *11*, 84. <https://doi.org/10.3390/aerospace11010084>

Academic Editor: Angelo Cervone

Received: 29 October 2023

Revised: 6 January 2024

Accepted: 8 January 2024

Published: 17 January 2024



Copyright: © 2024 by the authors. Licensee MDPI, Basel, Switzerland. This article is an open access article distributed under the terms and conditions of the Creative Commons Attribution (CC BY) license (<https://creativecommons.org/licenses/by/4.0/>).

1. Introduction

Miniaturization and improved performance of electronics, power systems, guidance, navigation and control devices on space systems have led to ever smaller and increasingly capable spacecraft. These technological improvements have translated into reduced mass and volume, resulting in significant launch cost savings. Smaller spacecraft are, therefore, becoming widespread platforms for interplanetary exploration, though they continue to face significant propulsion challenges limiting their current applications. State-of-the-art electrical propulsion technologies, such as ion propulsion, have been demonstrated, but with very low thrust levels [1]. Interplanetary exploration often requires a spacecraft to climb from a low orbit around another body to achieve escape velocities, and since ion thrusters provide values typically measured in milli-Newtons, such solutions require long mission times with careful and complex maneuvering. A more effective propulsion solution is thereby desired to enable interplanetary capability.

Figure 1 illustrates the concept of small spacecraft harvesting water from a low-gravity object such as an asteroid and using the water as fuel for interplanetary transit. Utilizing water from such sources allows a spacecraft to refuel without interaction with a moon or planet which have significant gravity potentials. Such a system would theoretically be capable of moving between the Earth and the asteroid belt using water from these sources [2].

In this paper, we present a solar thermal propulsion system capable of using non-purified water, possibly harvested from low-gravity objects such as near-earth asteroids [3,4], which incorporates focusing mirrors upon highly refractive materials to achieve fluid working temperatures as high as 4275 K [5]. At these temperatures, water experiences significant chemical decomposition into both molecular and monatomic components.

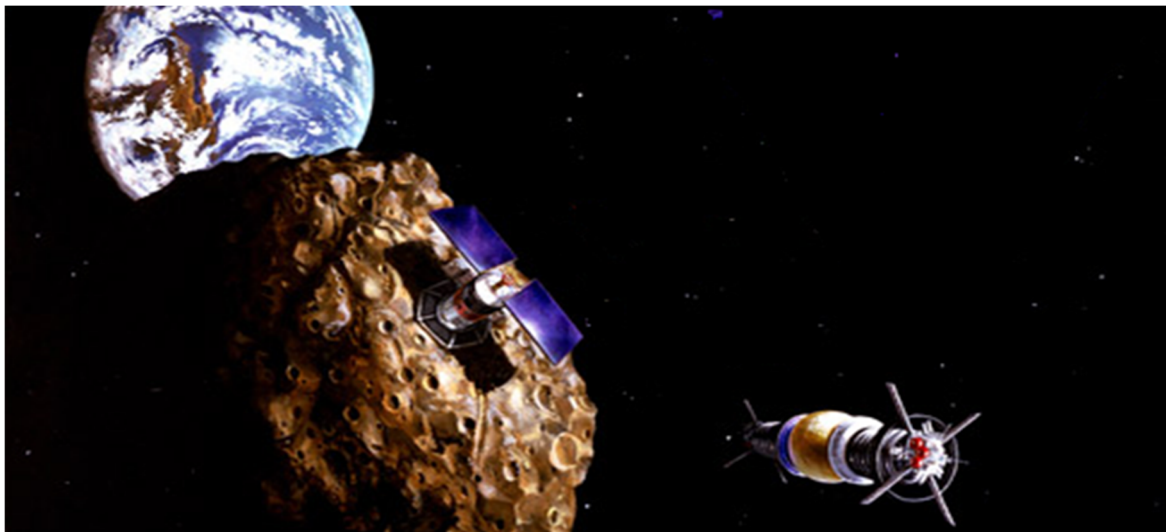


Figure 1. Water extracted from asteroids [3,4] and small bodies can be readily used as fuel in a solar thermal steam propulsion system (courtesy NASA).

These are very high-energy components, particularly the monatomic species of hydrogen and oxygen, and their formation enthalpies produce theoretical I_{sp} values higher than those for the classic cryogenic hydrogen-oxygen rocket motor. Specific Impulse, or I_{sp} , is a common metric for rocket motor propulsion. Specified with units of seconds, it provides the effective outgoing velocity of the exhaust gases when multiplied by g (9.806 m/s^2). In this work, we present a detailed explanation of such a solar-thermal propulsion concept, calculate its theoretical I_{sp} , and highlight how it could be implemented onto a demonstrator spacecraft.

Any technique for using water as a propellant must implement a power source sufficient to either heat water to useful propulsive temperatures or electrolyze water into its fuel and oxidizer components [6–8]. In our approach, we explore using solar concentrators, focusing power onto a chamber of a highly refractive material such as Tantalum Hafnium Carbide [5] to superheat working fluid temperatures to 4000 K.

Description of Proposed System

A deployable parabolic solar concentrator is envisioned [9,10], focusing solar energy onto a small spherical chamber. Liquid water is continuously injected into this spherical dissociation chamber, vaporizing and then heating it much further up to a nominal 4000 K working temperature. As shown qualitatively in Figure 2 (quantitative values are presented in Section 3.1), such high temperatures not only dissociate water molecules into molecular hydrogen and oxygen, but further dissociate much of the hydrogen and oxygen molecules into monatomic elements. Both of these steps take large amounts of energy (Figures 2 and 3), and the net result is a gas mixture within the dissociation chamber which has significantly more energy than temperature alone would indicate.

The resulting high energy gas mixture then escapes through the throat into a nozzle, where expansion will start to allow temperatures to drop. As temperatures drop, the equilibrium for the gas mixture shifts, allowing molecular hydrogen and oxygen to reform. Eventually further expansion allows them to recombine back into steam. All these reactions release heat, which slows the cooling of the gas as it expands, keeping temperatures high even while significant expansion is occurring in the nozzle. Only after temperatures have dropped back below 2000 K, does the nozzle revert to its conventional role of maximizing momentum transfer from a chemically stable exhaust gas mixture (superheated steam in this case). It is worth noting here that the autoignition temperature for a stoichiometric hydrogen/oxygen mix at one atmosphere is 839 K [11], meaning that combustion and/or dissociation occurs without an ignition source at our temperatures of interest.

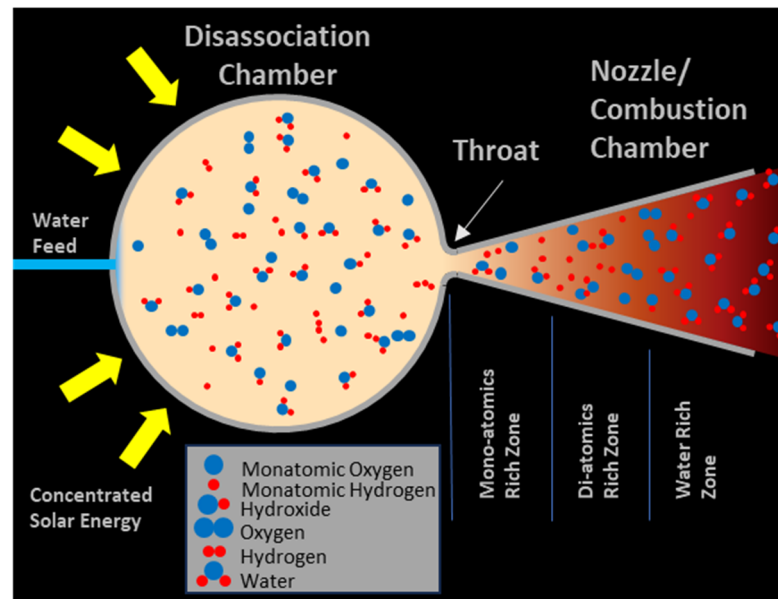


Figure 2. Thruster Concept: Water is dissociated in a chamber at very high temperatures, and then allowed to escape through a throat and combust downstream in a nozzle.

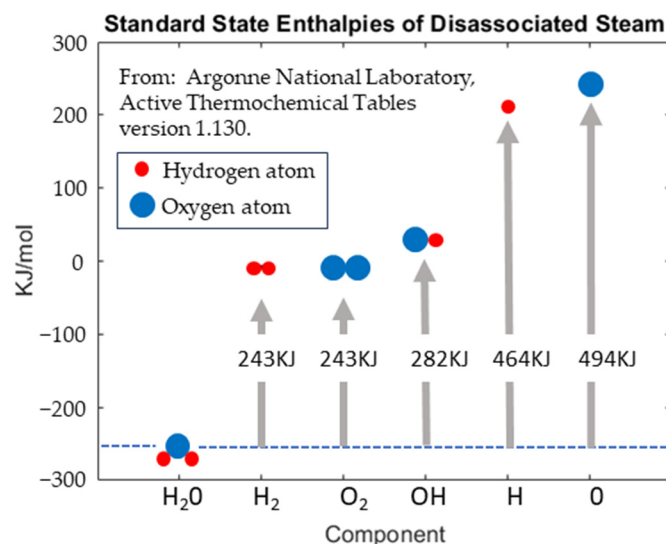


Figure 3. Enthalpies of Formation: Large amounts of energy are required to dissociate steam into Oxygen and Hydrogen components.

This proposed system, which appears conventional at first glance, is qualitatively different from a standard rocket motor because combustion occurs in the nozzle where the molecular components recombine into water, releasing energy as the gas expands as shown in Figure 3. Net combustion does not occur in the dissociation chamber because the gas mixture is in equilibrium, with dissociation and combustion occurring in equal amounts, resulting in the mole fractions documented by Ohta et al. [12], and shown in Figure 8. Temperatures up to 3500 to 4275 K appear feasible based upon the melting point of existing refractory metals such as Tantalum Hafnium Carbide [8], leading to theoretical I_{sp} values in the range of 450 s to 750 s (see Section 4) depending on chamber working temperatures and exhaust gas temperature.

Our proposed solar thermal steam propulsion system has four key characteristics. Firstly, the propellant is liquid water, safe, easy to store, and relatively low cost. Secondly, the propellant can be generated in-situ from asteroids or comets. Water for our proposed system does not have to be purified or distilled, and can be stored in bulk as a non-corrosive,

low-pressure liquid. Thirdly, this proposed technology utilizes reflected thermal energy directly from the Sun, unlike electric (or ion) propulsion, which uses photovoltaics which have conversion efficiencies limited to approximately 40% [13,14]. Fourthly, the proposed system can produce higher thrust than Hall effect ion engines, typically 80–200 mN [15], which is useful for shortening transit and maneuver times.

2. Background and Related Work

2.1. Thermal Rockets and Electrolyzing Systems

Thermal rockets, where a working fluid is heated to produce thrust, have a long history in rocket propulsion. Although relatively little activity has taken place in recent years, considerable efforts were executed post World War II, focusing on running liquid hydrogen over a high temperature nuclear reactor core and then out a conventional rocket nozzle. Although never flown, this technique claimed significant success in projects Rover, and its civilian successor, NERVA (shown in Figure 4) between the years 1955 and 1972. This technology is designed for high thrust boosters with an eye towards cryogenic single stage to orbit capability, and exhibited significant success, operating for minutes at a time at temperatures in the range of 2272 K to 2306 K [16], corresponding to theoretical I_{sp} of 700 s to 705 s respectively, using hydrogen as the working fluid and the calculation technique established in Section 3. Most recently, project DRACO, sponsored by DARPA and NASA, has resurrected this concept with the intent of providing considerable performance improvements for cis-lunar and interplanetary propulsion.

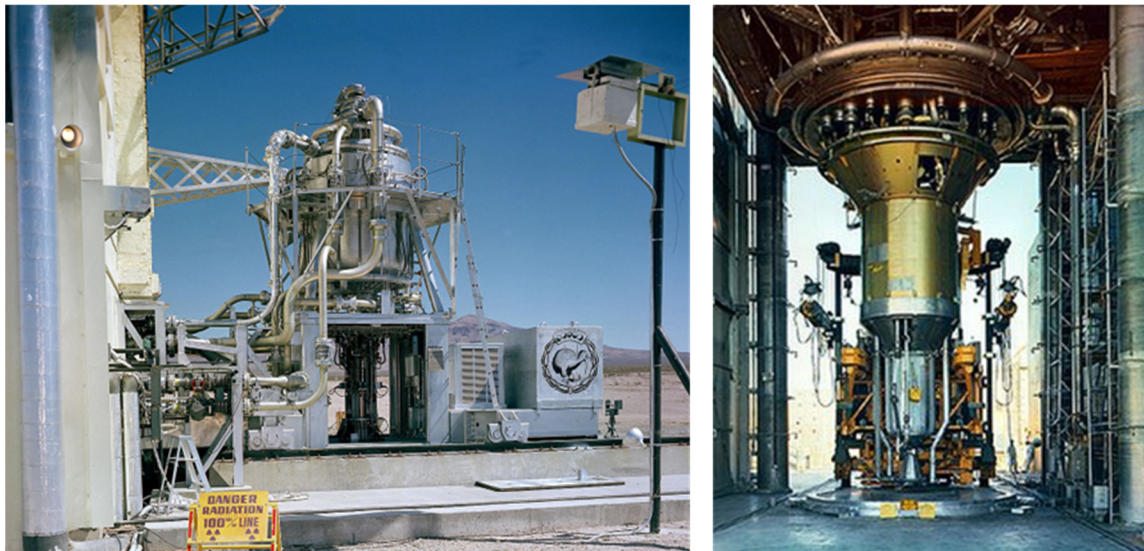


Figure 4. Projects Rover and NERVA: Nuclear powered test stands show prototypes of large scale nuclear powered thermal rockets (courtesy NASA).

2.2. Electrolyzing Systems

Electrolysis systems have been proposed, and recently system testing has taken place using platinum catalyst beds for ignition, demonstrating basic CubeSat-sized capability [17]. Given that such a system uses water as the working fluid, which is much easier to handle than hydrogen, and recent advances in electrolysis efficiency have produced values approaching 98% [18], this is a promising approach. However, extracted water would likely contain S- and C-bearing impurities, which may be harmful to water electrolyzers normally used to convert the water into hydrogen and oxygen. Proton Electron Membrane (PEM) water electrolyzers are also highly efficient, however the platinum catalysts used are subject to rapid degradation from trace quantities of sulfates and possibly carbon monoxide [19,20]. These impurities present challenges for electrolyzing extracted water.

2.3. Solar Thermal Technologies

The concept of using solar energy for power production is, of course, a long-accepted method for power production outside the Earth's atmosphere, where weather and attenuation are not issues. Around Earth, solar irradiance is 1365 W/m^2 , providing a ready source of reliable power. Solar thermal propulsion has received some significant research, including the Air Force Research Laboratory, with a report from 1981 providing an overview of plausible systems, again using hydrogen as a working fluid, with theoretical I_{sp} s of 872 s [21].

For a compact spacecraft, we propose parabolic collectors which focus the incoming solar flux onto the receiver point. Not all technologies are scalable in weight (or mass) for space applications. However, there is a way to modify the concentrator systems to make them scale well using inflatable systems [22,23]. These systems use minimal volume on launch, using compressed air for deployment once in space. Although inflatable Fresnel lenses have been used with success in space [24,25], their concentration ratio is not as attractive as membrane-type inflatable concentrators [22]. Stretched membranes for concentrating solar collectors offer the prospect of being very lightweight, structurally efficient, potentially low cost, and potentially similar in optical performance compared to the more conventional rigid glass/metal concentrator design approaches used in heliostat and parabolic dish applications (Figure 5).

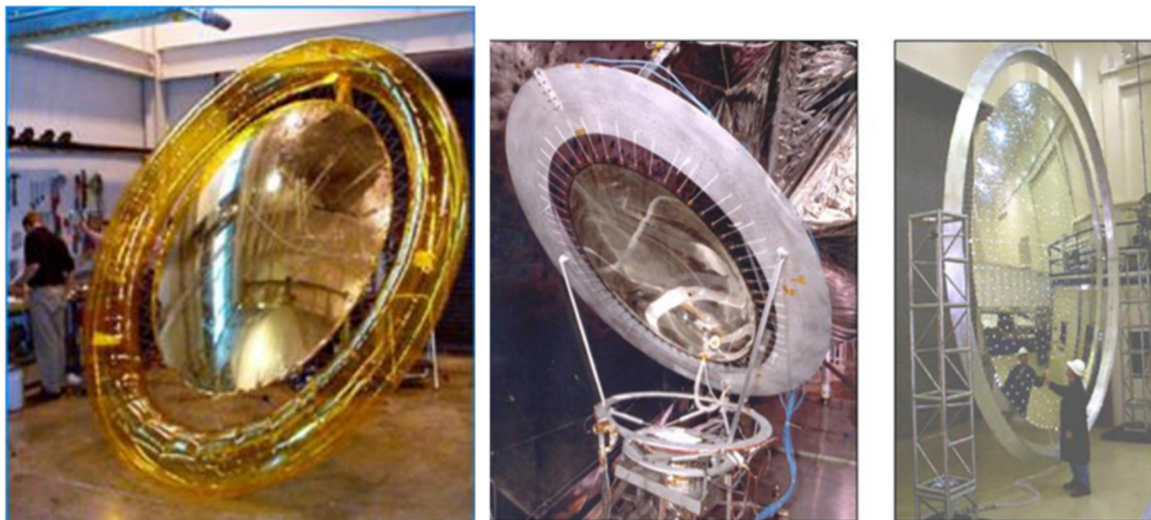


Figure 5. Space-based membrane concentration systems. Courtesy: NASA [5,8].

The potential reaction mass for solar thermal rockets could be extracted from near Earth asteroids. More than 75% of known asteroids are C-type. They have spectral characteristics similar to CI and CM carbonaceous chondrite meteorites, which are water rich, and so are thought to derive from such asteroids [19].

The physical design of solar concentrators to provide the necessary thermal power is another significant consideration for this concept. One idea considered was developed by AFRL (Air Force Research Laboratories) and Rockwell in 1979 involving large inflatable truss structures and reflectors (Figure 6) [26]. Another proposed system uses fiber-optics to collect the light and heat the propellant as shown in Figure 7 [27].

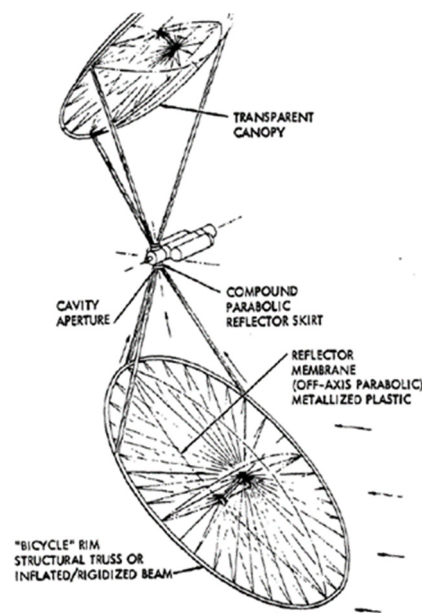


Figure 6. Solar thermal spacecraft design proposed in 1979 by AFRL and Rockwell International [25].

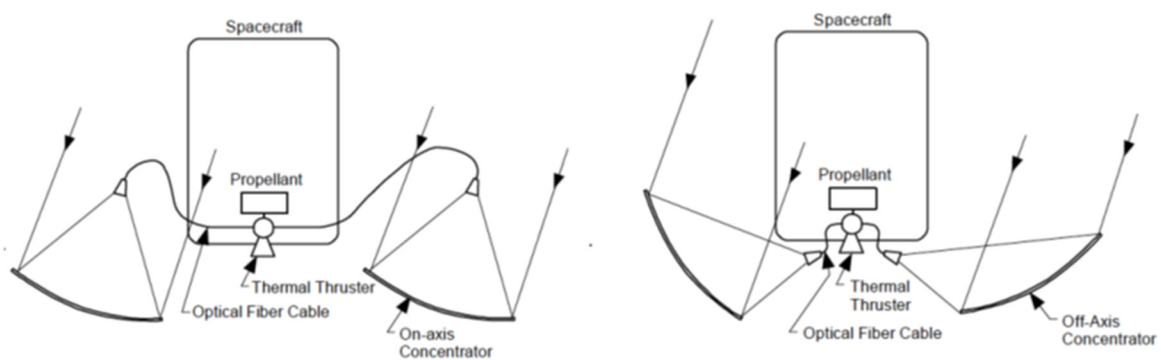


Figure 7. Fiber optic solar thermal configurations. On-axis (left) and off-axis (right) [26].

In 1996, Fortini et al. [28] proposed open cell foam to facilitate heat transfer, but because we propose temperatures as high as 4000 K, there are few plausible candidate materials for heat transfer at that temperature.

3. Method: Analysis of a Disassociated Steam System

In this design, to avoid a complicated solar concentrating system, we will define the primary component as a reflective mirror. Fresnel lenses are also plausible solar concentrators, however, are refractive lenses, incurring significant volume as well as requiring complex and expensive shapes. They are also subject to chromatic aberration, thus limiting their focusing performance. Parabolic mirrors are likely to be the best option for space applications, as they achieve the highest concentration ratios, are lightweight, and are simple.

The body of research investigating the dissociation of water at very high temperatures is relatively slim. It is dominated by analytical calculations since it is difficult to reach and stabilize at our operating temperature, much less make accurate measurements there. Fortunately, classical gas dynamics are relatively well established, and a body of literature exists exploring the dissociation of water at temperatures up to 5000 K, though mostly for the exploration of industrial scale hydrogen production. Ohta et al. [12] provides a chapter in their book on water splitting systems which serves as the primary source for calculations in this paper. Chialvo & Vlcek [29] provide a model, but present only some

selected parameters at temperatures no higher than 3500 K. Betelin et al. [30] propose modeling of a hydroxyl combustion process using the LOGOS code, but this would require both the code and the additional modifications for establishing the dynamics of dissociation, and this is similar to the limitations using the techniques given by L.M. Das [31], which works to model combustion dynamics. In this paper, we have utilized the molar fraction data from Ohta et al. [12] at 1 bar pressure as a baseline for our calculations.

3.1. Disassociative Steam Energy Calculations

3.1.1. Heat of Formation of Components

As previously shown in Figure 2, the dissociated steam components store significant amounts of energy. The standard enthalpy of formation for these dissociated components is defined as the change in enthalpy when one mole of a substance in the standard state (1 atm of pressure and 298.15 K) is formed from its pure elements under the same conditions [32]. The enthalpies used in our research are the standard state enthalpies of the dissociated components at standard conditions (temperature 298 K, pressure 1 atmosphere) found in Table 1 below for H₂O, HO, H, O, H₂, and O₂, respectively [33].

Table 1. Heat Capacities, Specific Heats, and Heat of Formation [32], of Components at T = 298 K.

	H ₂ O (g)	OH	H ₂	O ₂	H	O
γ	1.33	1.4	1.4	1.4	1.67	1.67
C_v [J/(mol K)]	25.18	20.76	20.76	20.76	12.4	12.4
$q(F)$ [kJ/mol]	−242	37.5	0	0	218	249

3.1.2. Specific Heat Capacities for Each Component

Because our dissociation chamber has a fixed volume, we calculate the specific heat capacities of each dissociated steam component under isochoric conditions. According to its unit J/mol·K, the specific isochoric heat capacity C_v tells us how much heat must be added or removed to or from one mole of a substance to increase or decrease, respectively, its temperature by one degree Kelvin under isochoric conditions [11]. In this Section, we present the isochoric specific heat capacity equation used to compute C_v for each of the dissociated components at various temperature states throughout the dissociation process:

$$C_v = (n * R) / (\gamma - 1) \quad (1)$$

where n is the number of moles of a dissociated steam component at a given temperature, R is the universal gas constant, 8.31 J/mol·K, and γ is the heat capacity ratio. Heat capacity ratios are a function of the number of atoms in the molecule, and are stated in Table 1.

3.1.3. Thermal Energy of Individual Components

The heat capacity ratio (γ) of components is specific to the types of gas, 1.33 for tri-atomic molecules (H₂O), 1.40 for diatomic molecules (OH, H₂, O₂), and 1.67 for monatomic (H, and O) gases. The consolidated calculations are presented below along with the heat capacities derived using Equation (7), and the standard state enthalpies at standard temperature and pressure, drawn from reference [33].

3.1.4. Component Dissociation as a Function of Temperature

As previously discussed, the existence of very high temperature materials such as Tungsten Hafnium Carbide provides an opportunity to raise the operating temperatures of gas generators to levels consistent with the disassociation of water into its component molecular and/or atomic components. Ohta et al. [12] detail how water breaks down at very high temperatures, showing significant disassociation occurs as temperatures rise. Here we choose a relatively low pressure of 1 bar because (1) materials at these high temperatures are expected to have low tensile strength, and (2) more dissociation

occurs at lower pressures. At 4000 K and 1 bar pressure, it can be seen in Figure 8 that most of the water has disassociated, and furthermore a significant fraction of the hot gas mixture is now comprised of monoatomic hydrogen and oxygen. The formation energies of these components provide a mechanism for storing energy, thus significantly boosting I_{sp} without commensurate temperature increase. Using the molar fraction data from Figure 8, we can calculate the total number of moles of each component that results from partial disassociation as a function of temperature. This step is necessary before we can calculate the total amount of energy present at a given temperature per kg of incoming fuel water.

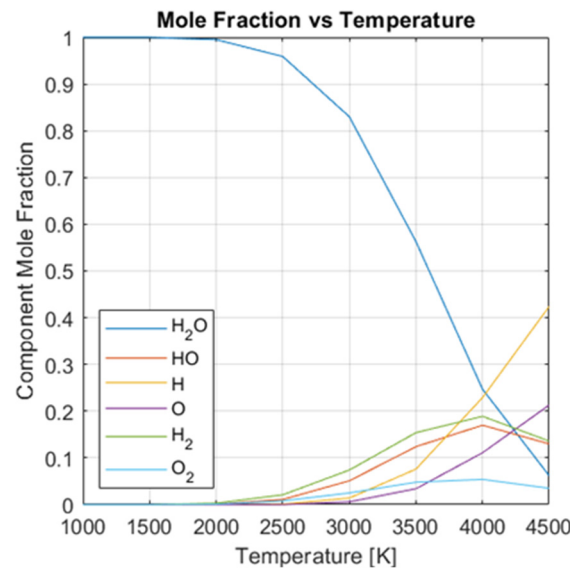


Figure 8. Dissociation molar fractions of water as function of temperature from Ohta et al. [12].

Reference [12] gives us the molar fraction of disassociated components as a function of temperature, but not the total number of moles in the heated mixture. One mole of water will eventually decompose into three moles total as temperatures rise, (two of atomic hydrogen, and one of atomic oxygen). To obtain individual mole levels from mole fractions, we start with a definition relating the original 1 mole of steam to some (as yet) unknown number of disassociated moles after heating given the total amount of material is conserved:

$$1 \text{ mole} \cdot m_{H_2O} = n_{H_2O}m_{H_2O} + n_{OH}m_{OH} + n_{H_2}m_{H_2} + n_{O_2}m_{O_2} + n_Hm_H + n_Om_O \quad (2)$$

where m_x is the molecular weight of each component, i.e., water, hydroxyl, diatomic hydrogen, oxygen, and finally monatomic hydrogen and oxygen. n_x is the corresponding number of moles of each of these components in the heated gas mixture assuming we started with 1 mole of water.

Define also:

$$n_t = n_{H_2O} + n_{OH} + n_{H_2} + n_{O_2} + n_H + n_O \quad (3)$$

where n_t is the total number of moles of the disassociated gas. This is 1 at low temperatures, and 3 at very high temperatures. We do not know n_t yet, but we can divide both sides of the above equation to get:

$$\frac{m_{H_2O}}{n_t} = \frac{n_{H_2O}}{n_t}m_{H_2O} + \frac{n_{OH}}{n_t}m_{OH} + \frac{n_{H_2}}{n_t}m_{H_2} + \frac{n_{O_2}}{n_t}m_{O_2} + \frac{n_H}{n_t}m_H + \frac{n_O}{n_t}m_O \quad (4)$$

Reference [12] gives us the molar fraction of each component as a function of temperature, thus we know n_{H_2O}/n_t etc., therefore the entire right side of the equation is known. As thus, we can solve directly for n_t :

$$n_t = \frac{m_{H_2O}}{\left(\frac{n_{H_2O}}{n_t} m_{H_2O} + \frac{n_{OH}}{n_t} m_{OH} + \frac{n_{H_2}}{n_t} m_{H_2} + \frac{n_{O_2}}{n_t} m_{O_2} + \frac{n_H}{n_t} m_H + \frac{n_O}{n_t} m_O \right)} \quad (5)$$

And now since we now know the total number of moles as well as the molar fractions for each molecular component, we can calculate the number of moles of each disassociated component as a function of temperature using the molar fraction:

$$n_{H_2O} = \left(\frac{n_{H_2O}}{n_t} \right) n_t \text{ etc } \dots \quad (6)$$

where n_{H_2O}/n_t is the known mole fraction from reference [12], and n_t is the total number of moles of disassociated gas in the mixture, having started with 1 mole of water at room temperature. This calculation for the rest of the components follows, repeating using their particular mole fraction values at that temperature. Figures 8 and 9 show the difference between mole fraction and actual molarity in the gas mixture as temperatures rise, starting with 1 mole of water at 1 bar atmospheric pressure. Note that components in the left chart sum to unity, while the right chart will eventually have a total of 3 moles, representing 1 mole of water dissociating into 2 moles of atomic hydrogen and 1 of atomic oxygen at very high temperatures.

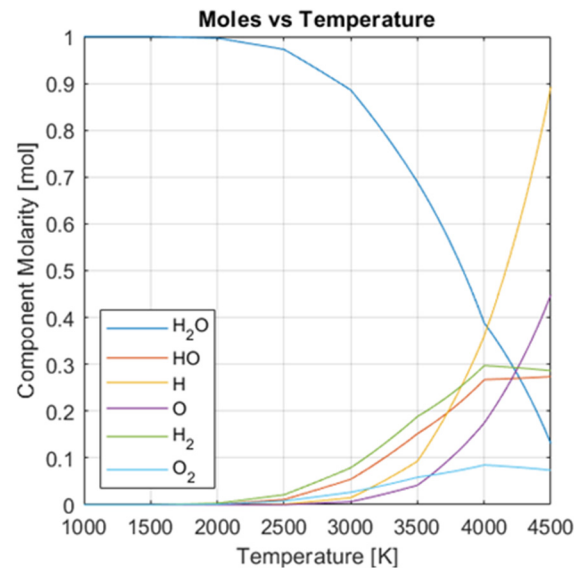


Figure 9. Resultant molar levels in gas mixture.

3.1.5. Total Thermal Energy as a Function of Temperature

Knowing the molar mixture as temperature rises now gives us the ability to calculate the total available energy q_{tot} for our I_{sp} calculation. Starting with one mole of water (vapor) at 298 K, the initial available energy is:

$$q_{H_2O}(T_{298}) = q_{H_2O(F)} + C_{v(H_2O)} T \quad (7)$$

where $q_{H_2O}(T_{298})$ is the available energy of one mole of steam at 298 K, $q_{H_2O(F)}$ is the formation heat for steam, $C_{v(H_2O)}$ is the constant volume heat capacity for steam, and T is the initial temperature (298 K in this case). The energy added to the system for each temperature step is thereafter a mixture of formation energies and component heat

capacities, proportional to the changing molar amounts in the chamber. Given we are starting with a mole of water, consistent with the previous Section, we have:

$$\begin{aligned} \frac{dq_{H_2O}}{dT}(T) &= (n_{H_2O}C_{v(H_2O)} + n_{OH}C_{v(OH)} + n_{H_2}C_{v(H_2)} + n_{O_2}C_{v(O_2)} + n_H C_{v(H)} + n_O C_{v(O)}) \dots \\ \dots + \left(\frac{dn_{H_2O}}{dT}\right)q_{H_2O(F)} &+ \left(\frac{dn_{OH}}{dT}\right)q_{OH(F)} + \left(\frac{dn_{H_2}}{dT}\right)q_{H_2(F)} + \left(\frac{dn_{O_2}}{dT}\right)q_{O_2(F)} + \left(\frac{dn_H}{dT}\right)q_{H(F)} + \left(\frac{dn_O}{dT}\right)q_{O(F)} \end{aligned} \quad (8)$$

This equation gives the derivative of energy as a function of temperature for one mole of steam as it disassociates. The top line of the equation is simply the energy gained given the current molar makeup of the disassociated gas mixture, but the second line represents the energy transfer resulting from the rates of chemical decomposition. Up to about 2000 K, this is simple, as there are no components in the heated mixture other than water. Higher temperatures, however, start to see disassociation, and then the formation of other components starts to become significant. From the previous Section, we know the number of moles in the mixture as a function of temperature, so we can take the numerical derivative with respect to temperature to get values for dn_{H_2O}/dT etc., and given the formation heats from the table above, we can integrate over temperature to get total available energy in the resulting gas mixture:

$$q_{total} = q_{H_2O}(T_{298}) + \int_{T_{298}}^{T_{final}} \frac{dq_{H_2O}}{dT}(T)dT \quad (9)$$

This gives the total available energy from an original mole of water heated up to temperature T_{final} , with units in $J \text{ mol}^{-1}$, which we can convert into total energy per kilogram (h_{total}) by dividing by the molecular weight of a water molecule (0.018 kg/mole). These results are shown in Figure 10, illustrating the steep increase in available energy at temperatures above 3000 K.

Available Energy (h_{total}) vs Dissociation Chamber Temperature

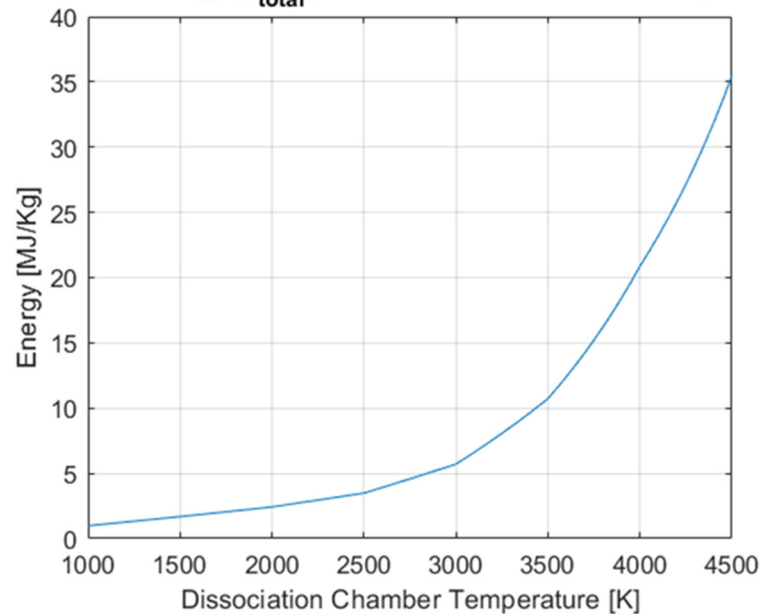


Figure 10. Total available energy at temperatures above 3000 K rapidly increases as steam dissociates into hydrogen and oxygen components.

3.2. Parabolic Concentrator Optics

A parabola is a curve that is defined as being the set of points that are equidistant from a fixed line, called directrix, and a fixed point, the focus. If the origin of the parabola is taken in the vertex, the equation of the parabola can be written as:

$$4fz = (x^2 + y^2) \quad (10)$$

where f is the distance between the vertex and the focus, and (z) is the optical axis. With this geometry, any incident ray parallel to the optical axis, will be reflected towards the focal point. In such a system, one can increase the mirror radius to capture and concentrate whatever power is required at the focal point. In reality, the sun's rays are not exactly coincident with the optical axis. Even in the ideal case of a perfectly formed mirror and perfect pointing, the angular extent of the sun itself limits the effective concentration of light rays by virtue of the fact that the incoming rays are emitted uniformly across the solar disc, which has an angular extent of about 9.31 milliradians when seen from the distance of the Earth's orbit, and this prevents the reflected energy from focusing down to a single point.

A simulation is therefore written to explore potential mirror designs for very high concentration ratios, randomly sampling incoming photons coming from the sun, and then reflecting them off a candidate mirror surface to establish whether they then strike the surface of the dissociation chamber which is located at the focal point. In general, as the distance from the mirror surface to the dissociation chamber increases, the farther the incoming ray will diverge, eventually missing the chamber completely. Figure 11 shows a mirror large enough to illustrate this effect, with rays further out from the center axis having a longer distance to travel, hence a higher probability of not hitting the chamber.

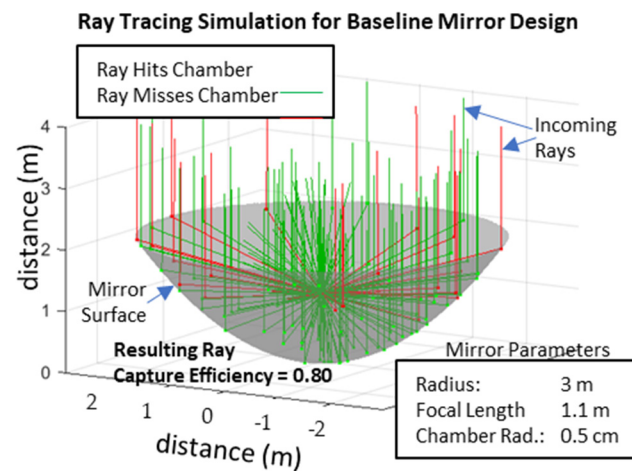


Figure 11. Ray tracing simulation is used to statistically establish the efficiency of solar concentration as mirror sizes increase.

Given some basic parameters for the system, a rough optimization of the mirror can be achieved by varying mirror radius and focal distance. We then calculate whether the resulting power received by the dissociation chamber is sufficient to maintain our nominal operating temperature and propellant flow rate. This must be done to ensure that a mirror system exists which is capable of the extreme heating needed by our proposed propulsion system. Given a first order baseline of a dissociation chamber with a 5 mm radius, we assume an emissivity of 0.9, an input water mass flow of 1 g/s and calculate the net power received by the dissociation chamber for a perfect parabolic reflector. An operating temperature of 4000 K is also assumed, which allows us to calculate the chamber blackbody emissions of the 0.5 cm radius sphere to be 4.1 kW. We vary mirror radius and focal length and then use the simulation to calculate the resulting net power input, which must be

higher than 21.2 kW for our chosen mass flow rate, as calculated by the techniques detailed in Section 3.1.

Smaller mirrors have smaller distances to the focal point, and thus transfer all incoming energy to the chamber, hence the identical parabolic curves for lower mirror radii. As radius and focal length increase, some of the power is lost because some rays will not reflect onto the chamber, even as total power continues to increase. Simulation results, shown in Figure 12, indicate that a mirror radius near 3 m with a focal length of 1.1 m is capable of projecting adequate power to the dissociation chamber to reach 4000 K with a fuel flow rate of 1 g/s.

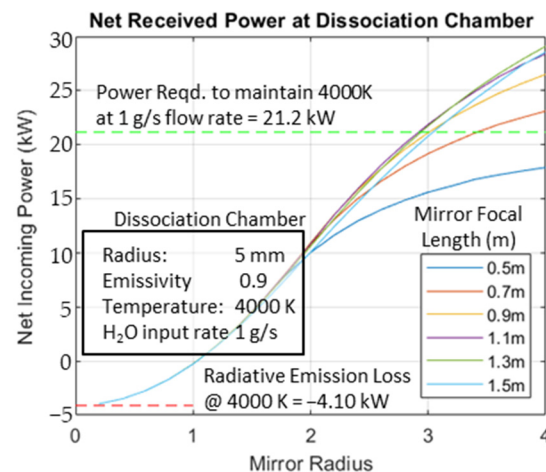


Figure 12. Simulation results indicate that a 3 m mirror provides adequate power for a 0.5 cm radius dissociation chamber.

3.3. Parabolic Concentrator Configurations

In its basic form, a parabolic concentrator is a single parabolic mirror, focusing the sun's rays on the chosen receiver. It focusses the light by 'reflecting' it onto the receiver. Such a system is well established and easily analyzed. Alternatively, a Cassegrain approach (Figure 13) can be implemented, allowing the target to be moved out of the sunlight, and possibly implementing gimbaling to change thrust direction. While parabolic concentrators focus the light by 'reflecting' it onto the receiver. When pointing away from the sun, the configuration shown in Figure 14 could be used. The achievable concentration ratio when the spacecraft moves towards the sun, depends on the extended mirrors. While moving towards the sun the reflective mirrors focus the light by 'reflecting' it onto the parabolic concentrator and then reflecting on the receiver. This system is similar to a solar furnace. The additional reflection from the mirrors to the parabolic concentrator are the primary reflection losses. These losses can be minimized by using highly reflective smooth aluminum sheets which reflect more than 95% of light [34]. A smooth surface will also ensure specular reflection of light with very low diffusion. Such losses directly affect the temperature of the receiver. This will in turn reduce specific impulse and thrust generated.

Direct solar collection ensures that heat focuses onto the disassociation chamber thus increasing efficiency. The elimination of heat exchangers simplifies the system design while also reducing the mass of the spacecraft. A parabolic dish (point heater) is preferred to a parabolic trough (linear heating) to achieve the high concentration ratios needed to achieve high receiver temperatures. The sunlight incident on the collector is converted to heat. The intensity of this heat depends on the concentration ratio of the mirror system. In the case of indirect heating methods, this heating is normally stored in a heat exchanger or thermal storage material, so the propellant is heated on demand. Direct methods, on the other hand heat the propellant without intermediate storage material. It should be noted that the only thermal losses in this method are radiative thermal losses from the dissociation chamber. If an indirect system with heat exchangers is used, losses would include radiative losses to

the surrounding space as well as thermal energy storage losses. This system increases the overall mass of the spacecraft, hence our preference for direct heating.

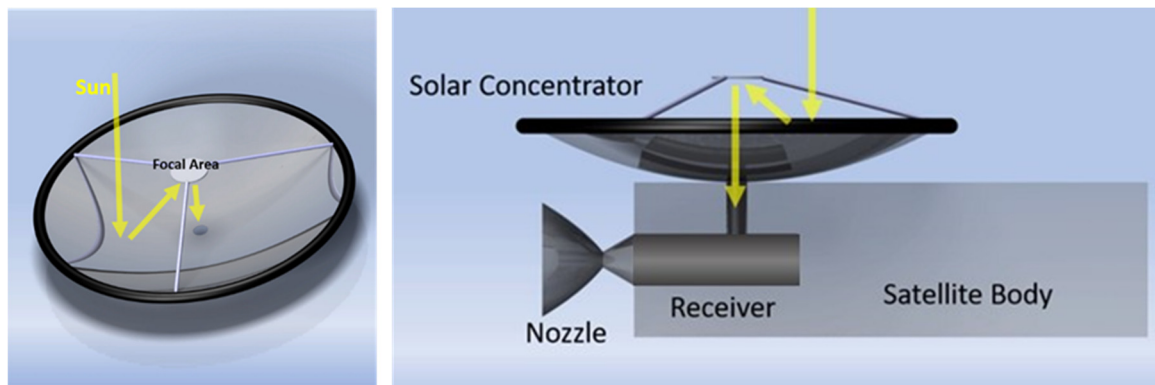


Figure 13. (Left) Solar Concentrator Concept. (Right) Direct-Gain Solar Thermal Steam Propulsion Concept.

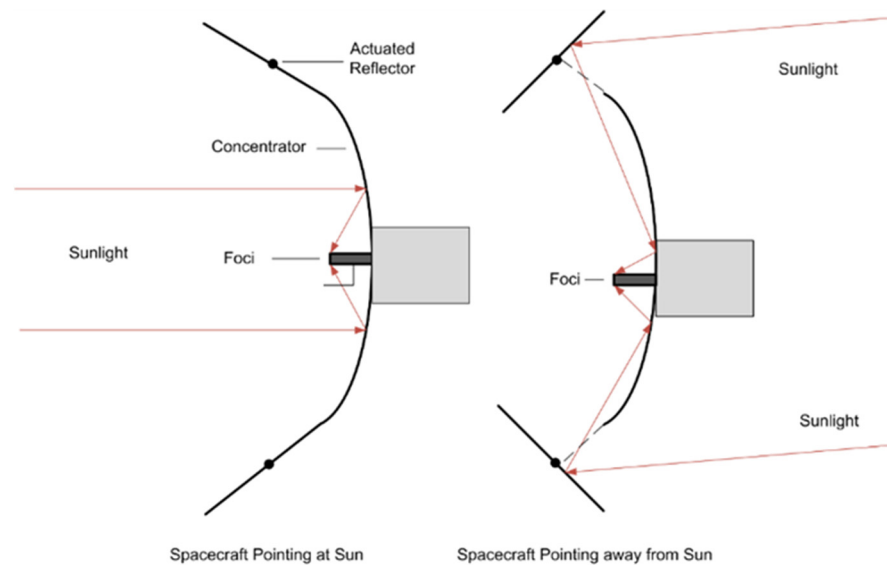


Figure 14. A solar thermal steam propelled spacecraft concept uses a series of actuated reflectors to concentrate sunlight when it is pointing away from the Sun.

4. Results

4.1. Specific Impulse Upper Limit Calculation

In the absence of a complex computational fluid dynamics model for high temperature steam expansion [35], the upper limit of I_{sp} can be calculated by equating total available heat energy in a gas mixture to kinetic energy as shown in reference [36]:

$$V_e = \sqrt{2(h_{total} - h_e)} \quad (11)$$

where V_e is the effective exit velocity of the gas out of the back of the nozzle, h_{total} is the total amount of energy per unit mass of the dissociated gas as it enters the nozzle throat, and h_e is the energy per unit mass of the water vapor at the exit plane of the nozzle. Note here that h and q are related by the molecular weight of water, i.e., $h_{total} = q_{total}/m_{H_2O}$ and $h_e = q_e/m_{H_2O}$ respectively. Given the definition of specific impulse, we can state that: $V_e = g I_{sp}$, where g is 9.81 m s^{-2} , and can thus substitute and solve for I_{sp} giving:

$$I_{sp} = \frac{\sqrt{2(h_{total} - h_e)}}{g} \quad (12)$$

Here we make the assumption that gas exits the nozzle at a variety of temperatures ranging from 298 K to 1000 K to establish h_e , bounding performance with a range of nozzle efficiencies pending a more detailed analysis of the combustion dynamics in the nozzle. The results of this calculation, shown for dissociation chamber operating temperatures from 1000 K up to 4500 K and nozzle exit temperatures from 298 K to 1000 K are shown in Figure 15. This gives us a specific impulse range of 643 s to 659 s for a dissociation chamber operating temperature of 4000 K. This can be directly compared to the theoretical specific impulse of a hydrogen/oxygen rocket motor by using the formation energies of non-cryogenic H_2 and O_2 respectively and applying the identical I_{sp} calculation technique from above assuming a stoichiometric mixture, the identical nozzle exit temperatures, and the formation heats for H_2 , O_2 and H_2O respectively. Doing this calculation results in a comparative theoretical specific impulse range of 509 s to 529 s for a hydrogen/oxygen rocket motor. The theoretical values for our proposed dissociated steam concept are thus higher because of the presence of monatomic hydrogen and oxygen in the gas mixture, and the extra energies of formation these species provide.

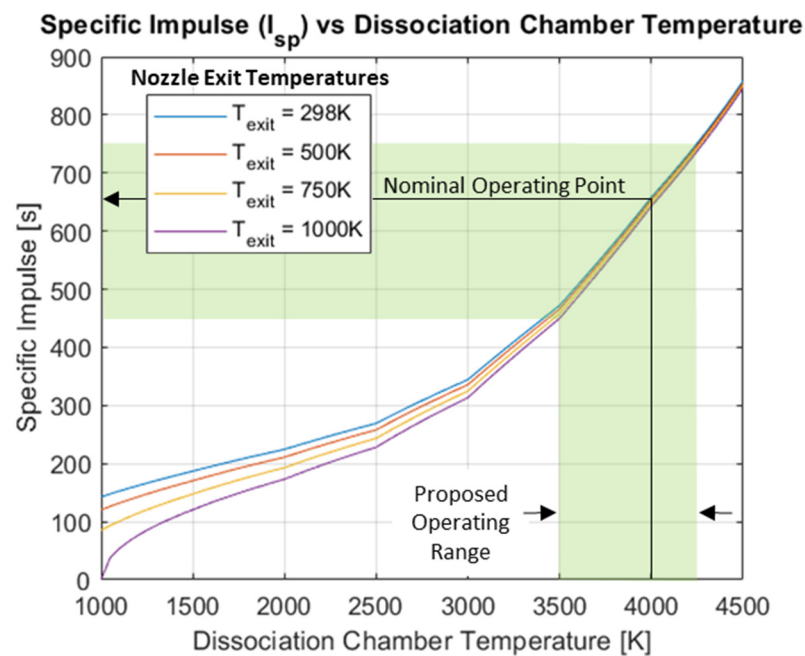


Figure 15. Specific Impulse for a dissociated steam propulsion system is limited by the maximum temperature of the dissociation chamber.

Finally, we can use the rocket equation to calculate the thrust for our nominal 1 g/s propellant flow rate:

$$Thrust = \dot{m}gI_{sp} = (0.001 \text{ kg/s}) (9.81 \text{ m/s}^2)(663 \text{ s}) = 6.50 \text{ N} \quad (13)$$

This indicates at least an order of magnitude or more of increased thrust levels relative to Hall effect thrusters which vary between 80–200 mN in thrust [15].

4.2. Propulsive Effectiveness at Increasing Distances from the Sun

Parameters for the above-described system are sized for the solar irradiance at Earth's orbit. The performance of a solar powered dissociative steam system necessarily declines as the distance from the sun increases. Given we wish to keep the operating temperature at 4000 K, we can decrease the mass flow rate of water as distance to the sun increases, thus maintaining specific impulse at the cost of reduced thrust, at least up to the distance where the solar concentrator can no longer maintain temperature, even for zero flow rate.

As distance from the sun increases, irradiance goes down as the reciprocal of the distance squared, but this is partially compensated for by the angular extent of the sun

becoming smaller, which improves focus, and thus mirror efficiency. The net effect of these two combined is shown in Figure 16, which details operating performance as a function of propellant mass flow rate as well as distance from the sun.

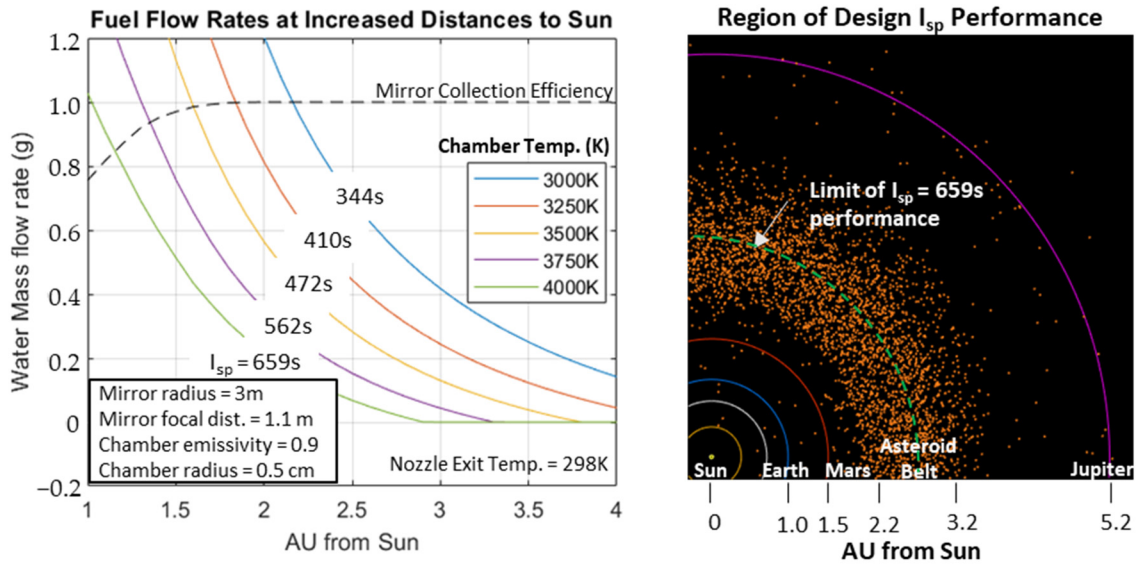


Figure 16. The proposed system can maintain high I_{sp} performance at up to 2.8 AU by reducing the flow of input propellant water, and exhibits graceful degradation at higher distances.

In general, a user can reduce the flow rate of the propellant to increase the dissociation chamber temperature, but this only works if there is enough power to overcome the radiant emissions of the chamber itself. For the baseline system described above, the optimal 4000 K operating temperature can be maintained up to about 2.8 AU, which means that an I_{sp} of 643 s to 659 s can be maintained up through the middle of the asteroid belt, with modest degradation up through 3.2 AU, which is the conventional end of the main asteroid belt. Larger flow rates can always produce additional thrust, just at lower I_{sp} values due to lower chamber temperatures. The overall effect is that of a system which shows graceful degradation from the power reduction up through the top of the asteroid belt.

4.3. Efficiency Comparison with an Electrolyzed Water System

It is useful to compare the efficiency of our proposed system with a more conventional electrolyzed water approach. Disregarding the power loss from nozzle expansion on both systems, we can compare the thrust and I_{sp} of each system as both methods use water as the input fuel.

For our proposed system, we establish the dissociative steam efficiency as:

$$\epsilon_{dissoc} = \frac{P_{output}}{P_{input}} = \frac{I_{solar} a_m \rho_s \epsilon_m e_{dc} - a_{dc} e_{dc} \sigma T^4}{I_{solar} a_m} \quad (14)$$

where ϵ_{dissoc} is the efficiency of the dissociative steam system, P_{output} is the kinetic power of the output thrust, and P_{input} is the total solar power passing through the entrance aperture of the solar concentrator. Accordingly, let us define the input power as the product of solar irradiance, I_{solar} , with mirror aperture area a_m . The amount of power striking the dissociation chamber is decremented by the fraction of power reflected specularly by the mirror, ρ_s , and then by the mirror efficiency, ϵ_m , which accounts for the fraction of rays which cannot be focused due to the angular extent of the sun (Section 3.3). Finally, the fraction of photons absorbed by the dissociation chamber is given by its emissivity, e_{dc} . This total input power must now be reduced by the self-emissions of the dissociation chamber at the chosen operating temperature, T , using the Stefan-Boltzmann law where a_{dc} is the

surface area of the dissociation chamber, e_{dc} (again), is the emissivity and σ is the Stefan-Boltzmann constant. We assume a perfect nozzle for the purposes of this comparison.

Choosing 1 AU as our distance from the sun, the solar irradiance is 1361 W/m^2 . The subtended area of the concentrator mirror, derived from its 3 m radius is 28.3 m^2 , and we will assume the mirror provides a specular reflection coefficient of 0.99. The mirror efficiency is 0.75, as derived from Figure 16, and we assume a dissociation chamber emissivity of 0.9. Using a 5 cm radius for the dissociation chamber, we can calculate its spherical surface area of 3.14 cm^2 , and using the operating temperature of 4000 K, the Stephan-Boltzmann equation provides total radiant emittance to be 4.10 kW. The approximate net efficiency of the disassociated steam system is thus:

$$\varepsilon_{ds} = \frac{\left(1361 \frac{\text{W}}{\text{m}^2}\right) (28.3 \text{ m}^2) (0.99) (0.75) (0.9) - \left(3.14 \times 10^{-4} \text{ m}^2\right) (0.9) \left(5.67 \times 10^{-8} \frac{\text{W}}{\text{m}^2 \text{K}^4}\right) (4000 \text{ K})^4}{\left(1361 \frac{\text{W}}{\text{m}^2}\right) (28.3 \text{ m}^2)} = 56.1\% \quad (15)$$

Alternatively, we can also establish the efficiency of an electrolytic system. Here we assume that electrical power generated by a photo-voltaic solar cell array with known input area a_{sc} to be a known fraction ρ_{sc} of the total solar irradiance I_{solar} collected. Multiplying the resulting electrical power by the efficiency of the electrolyzer, ρ_e . Assuming as before a perfect nozzle efficiency for comparison purposes with the dissociative steam system, we have

$$\varepsilon_{elec} = \frac{I_{solar} a_{sc} \rho_{sc} \rho_e}{I_{solar} a_{sc}} = \rho_{sc} \rho_e \quad (16)$$

In order to make a reasonable comparison, we assume that the solar panel area is identical to the solar concentrator aperture used by the dissociative system, 28.3 m^2 . From references used above in Section Description of Proposed System, we know that solar cell efficiencies approach 40%, and research on water electrolyzation techniques has recently demonstrated efficiencies up to 98% [18] using capillary-fed electrolysis cells. We therefore have:

$$\varepsilon_{elec} = (0.4)(0.98) = 39\% \quad (17)$$

This assumes that we do not store the propellant cryogenically, but take the gases as they are produced for combustion, allowing us to store propellant as water in a manner similar to the disassociated steam system as proposed. Comparing the two systems, dissociative steam remains considerably more efficient even assuming the near perfect electrolysis efficiencies demonstrated in recent years.

5. Discussion

In this paper, we propose the use of solar concentration to heat water to temperatures of 4000 K or more. The resulting high energy molecular mixture is used to generate modest amounts of thrust, on the order of single digit Newtons, with specific impulses at or above historically demonstrated levels for bipropellant systems. Direct solar heating has been shown to have significant potential to reach the concentration levels necessary to reach these extreme temperatures.

Our design approach shows how we can use solar concentrators to achieve high specific impulses, while allowing the spacecraft to move in any direction (Figures 13 and 14) using an array of add-on reflector mirrors. To date, there has been limited work in developing solar thermal concentrators in space. In fact, previous work focused on developing component technologies, including techniques for deploying large structures. Our approach shows that solar thermal heating technology is promising. For example, theoretical specific impulses of over 600 s can be achieved for solar powered systems using water as a working fluid.

Our work shows that monopropellant steam propulsion could be theoretically superior to a hydrogen/oxygen rocket motor in terms of I_{sp} performance, but without the complexity of bipropellant storage and plumbing. When compared directly with hydrogen/oxygen

rocket motors, this system does not require pressurized cryogenics, and can store the inert propellant as a liquid at standard pressure and temperature.

The big return on investment of this technology comes when solar thermal propulsion is coupled with ISRU (In Situ Resource Utilization), a key to enabling sustainable space exploration and transportation. Water is identified as the principal resource for making ISRU practical, both on asteroid/small bodies, the Moon, and Mars. The presented solar thermal propulsion technology does not face this challenge of impurity poisoning and is fundamentally simpler. However, solar thermal propulsion faces a major unknown, primarily the ability of suitable refractive materials to act as (even a modest) pressure vessel at temperatures approaching 4000 K. Plausibly, a solution can be engineered to mitigate and quantify this unknown, perhaps imposing lower performance bounds on the proposed system. It should be noted that solar thermal propulsion is still in its infancy, but represents perhaps the simplest method to utilize in-situ resources from C-class asteroids and small bodies.

6. Conclusions

In this work we have proposed and analyzed the feasibility of a solar thermal propulsion system. The concept uses water as the propellant which simplifies storage and facilitates ISRU. The technology utilizes parabolically concentrated solar energy to heat water into steam and then to temperatures approaching 4000 K. Solar energy can be absorbed with high efficiency, with refractive materials having emissivities of approximately 90%, which is a substantial improvement over photovoltaics that typically convert less than 40% of solar irradiance into electric power. In addition, theoretical I_{sp} is considerably higher for the dissociative approach ($I_{sp} = 643$ s to 659 s) relative to the standard hydrogen/oxygen rocket motor ($I_{sp} = 509$ s to 529 s) because significant energy is stored in the monatomic hydrogen and oxygen species.

The proposed system also produces higher thrust than electric thrusters, which is critical for getting into capture orbit and making planetary escape maneuvers within a reasonable time frame. Overall, the system is simple, contains minimal moving parts and shows performance comparable or superior to bi-propellant propulsion systems.

Author Contributions: Conceptualization, L.V. and J.T.; methodology, L.V., S.R., G.L., A.E. and J.M.D.; software, L.V., S.R., G.L., A.E. and J.M.D.; validation, L.V., S.R. and J.M.D.; formal analysis, L.V. and J.M.D.; investigation, L.V., S.R. and J.M.D.; resources, J.T.; data curation, L.V. and S.R.; writing—original draft preparation, S.R. and L.V.; writing—review and editing, L.V., S.R. and J.M.D.; visualization, L.V., J.T. and S.R.; supervision, J.T. and L.V.; project administration, J.T.; funding acquisition, J.T. All authors have read and agreed to the published version of the manuscript.

Funding: This research was funded by the National Aeronautics and Space Administration grant 80NSSC19M0197.

Data Availability Statement: The data presented in this study are available on request from the corresponding author.

Acknowledgments: We would like to thank Laurence Garvie, ASU Center for Meteorite Studies for helpful discussions, comments, and suggestions.

Conflicts of Interest: The authors declare no conflict of interest.

References

1. Rafalskiy, D.; Martínez, J.M.; Habl, L.; Zorzoli Rossi, E.; Proynov, P.; Boré, A.; Baret, T.; Poyet, A.; Lafleur, T.; Dudin, S.; et al. In-orbit demonstration of an iodine electric propulsion system. *Nature* **2021**, *599*, 411–415. [[CrossRef](#)] [[PubMed](#)]
2. Rabade, S.; Barba, N.; Garvie, L.; Thangavelautham, J. The Case for Solar Thermal Steam Propulsion System for Interplanetary Travel: Enabling Simplified ISRU Utilizing NEOs and Small Bodies. In Proceedings of the 67th International Astronautical Congress, Guadalajara, Mexico, 26–30 September 2016.
3. Beck, P.; Eschrig, J.; Potin, S.; Prestgard, T.; Bonal, L.; Quirico, E.; Schmitt, B. Water abundance at the surface of C-complex main-belt asteroids. *Icarus* **2021**, *357*, 114125. [[CrossRef](#)]

4. Rivkin, A.S.; Davies, J.K.; Johnson, J.R.; Ellison, S.L.; Trilling, D.E.; Brown, R.H.; Lebofsky, L.A. Hydrogen concentrations on C-class asteroids derived from remote sensing. *Meteorit. Planet. Sci.* **2003**, *38*, 1383–1398. [[CrossRef](#)]
5. Cedillos-Barraza, O.; Manara, D.; Boboridis, K.; Watkins, T.; Grasso, S.; Jayaseelan, D.D.; Konings, R.J.M.; Reece, M.J.; Lee, W.E. Investigating the highest melting temperature materials: A laser melting study of the TaC-HfC system. *Sci. Rep.* **2016**, *6*, 37962. [[CrossRef](#)] [[PubMed](#)]
6. Gabrielli, R.A.; Herdich, G. Review of Nuclear Thermal Propulsion Systems. *Prog. Aerosp. Sci.* **2015**, *79*, 92–113. [[CrossRef](#)]
7. Cheah, K.H. *Space Micropropulsion for Nanosatellites: Progress, Challenges and Future*; Elsevier: Amsterdam, The Netherlands, 2022.
8. Pothamsetti, R.; Thangavelautham, J. Photovoltaic Electrolysis Propulsion System for Interplanetary CubeSats. In Proceedings of the IEEE Aerospace Conference 2016, Big Sky, MT, USA, 5–12 March 2016.
9. Brandhorst, H.; Rodiek, H.A.; O'Neill, M.J.; Eskenazi, M. Ultralight, Compact, Deployable, High Performance Solar Concentrator Array for Lunar Surface Power. In Proceedings of the 4th International Energy Conversion Engineering Conversion and Exhibit, San Diego, CA, USA, 26–29 June 2006.
10. Wassom, S.R. Focus Control System for Solar Thermal Propulsion. In Proceedings of the International Adams User Conference, Rome, Italy, 15–17 November 2000.
11. *Glenn Safety Manual—Chapter 6: Hydrogen*; NASA Document No.: GLP-QS-8715.1.6; NASA: Washington, DC, USA, 2021; p. 8.
12. Ohta, T. (Ed.) *Solar-Hydrogen Energy Systems: An Authoritative Review of Water-Splitting Systems by Solar Beam and Solar Heat: Hydrogen Production, Storage, and Utilisation*; Pergamon Press: Oxford, UK, 1979.
13. Available online: <https://technology.nasa.gov/patent/LEW-TOPS-50> (accessed on 1 September 2023).
14. Li, J.; Aierken, A.; Liu, Y.; Zhuang, Y.; Yang, X.; Mo, J.H.; Fan, R.K.; Chen, Q.Y.; Zhang, S.Y.; Huang, Y.M.; et al. A Brief Review of High Efficiency III-V Solar Cells for Space Application. *Front. Phys.* **2021**, *8*, 631925. [[CrossRef](#)]
15. Tajmar, M. *Advanced Space Propulsion Systems*; Springer Nature: Berlin/Heidelberg, Germany, 2012; p. 76.
16. Finseth, J.L. *Rover Nuclear Rocket Engine Program: Overview of Rover Engine Tests*; NASA: Washington, DC, USA, 1991.
17. Hwang, M.; Rho, T.-S.; Lee, H.J. Conceptual design and performance analysis of water electrolysis propulsion system with catalytic igniter for CubeSats. *Acta Astronaut.* **2022**, *200*, 316–328. [[CrossRef](#)]
18. Hodges, A.; Hoang, A.L.; Tsekouras, G.; Wagner, K.; Lee, C.-Y.; Swiegers, G.F.; Wallace, G.G. A high-performance capillary-fed electrolysis cell promises more cost-competitive renewable hydrogen. *Nat. Commun.* **2022**, *13*, 1304. [[CrossRef](#)] [[PubMed](#)]
19. Bottke, W.; Cellino, A.; Paolicchi, P.; Binzel, R. *Asteroids III*; University of Arizona Press: Tucson, AZ, USA, 2002.
20. Thangavelautham, J. and Dubowsky, S. On the Catalytic Degradation in Fuel Cell Power Supplies for Long-Life Mobile Field Sensors. *J. Fuel Cells Fundam. Syst.* **2013**, *13*, 181–195. [[CrossRef](#)]
21. Air Force Research Labs Report: The Place of Solar Thermal Rockets in Space, C.C. Selph. May 1981. Available online: <https://apps.dtic.mil/sti/tr/pdf/ADA407602.pdf> (accessed on 1 September 2023).
22. Grossman, G.; Williams, G. Inflatable Concentrators for Space Propulsion and Dynamic Space Power. *J. Sol. Energy Eng.* **1990**, *112*, 229. [[CrossRef](#)]
23. Jenkins, C. Gossamer Spacecraft: Membrane and Inflatable Structures Technology for Space Applications. *Mech. Eng.* **2001**, *123*, 82.
24. O'Neill, M.J. Inflatable Fresnel Lens Solar Concentrator for Space Power. U.S. Patent 6,111,190, 29 August 2000.
25. NASA SBIR Directorate: Deployable Collectors for Advanced Space Power and Propulsion Systems. Glenn Research Center. 1997. Available online: <http://sbir.nasa.gov/SBIR/successes/ss/3-090text.html> (accessed on 1 September 2023).
26. Ethridge, F.G. *Solar Rocket System Concept Analysis*; Rockwell International Final Report, AFRPL-TR-79-79; Rockwell International, Space Systems Group: Downey, CA, USA, 1979.
27. Nakamura, T.; Sullivan, D.; McClanahan, J.; Shoji, J.M.; Partch, R.; Quinn, S. Solar Thermal Propulsion for Small Spacecraft. In Proceedings of the 41st ASME/ASME/SAE/ASEE Joint Propulsion Conference, Tucson, AZ, USA, 10–13 July 2005.
28. Fortini, A.; Tuffias, R.H. Design and Fabrication of Solar-Thermal Propulsion System. *AIP Conf. Proc.* **1996**, *361*, 1447.
29. Chialvo, A.A.; Vlcek, L. Behaviour of rarified steam at very high temperature an orientation-averaged interaction potential approach towards its accurate description. *Mol. Phys.* **2019**, *117*, 3922–3940. [[CrossRef](#)]
30. Betelin, V.B.; Shagaliev, R.M.; Aksenov, S.V.; Belyakov, I.M.; Deryugin, Y.N.; Korchazhkin, D.A.; Kozelkov, A.S.; Nikitin, V.F.; Sarazov, A.V.; Zelenskiy, D.K. Mathematical simulation of hydrogen–oxygen combustion in rocket engines using LOGOS code. *Acta Astronaut.* **2014**, *96*, 53–64. [[CrossRef](#)]
31. Das, L.M. Hydrogen-oxygen reaction mechanism and its implication to hydrogen engine combustion. *Int. J. Hydrogen Energy* **1996**, *21*, 703–715. [[CrossRef](#)]
32. Braeuer, A. *In Situ Spectroscopic Techniques at High Pressure*; Elsevier: Amsterdam, The Netherlands, 2015; pp. 49–192.
33. Argonne National Laboratory, Active Thermochemical Tables Version 1.130. Available online: <https://atct.anl.gov/Thermochemical%20Data/version%201.130/index.php> (accessed on 1 September 2023).
34. Schürmann, M.; Schwinde, S.; Jobst, P.; Stenzel, O.; Wilbrandt, S.; Yulin, S.; Szeghalmi, A.; Bingel, A.; Munzert, P.; Kaiser, N. High-reflective coatings for ground and space based applications. In Proceedings of the International Conference on Space Optics, Tenerife, Spain, 7–10 October 2014.

-
35. Varga, S.; Soares, J.; Lima, R.; Oliveira, A.C. On the selection of a turbulence model for the simulation of steam ejectors using CFD. *Int. J. Low-Carbon Technol.* **2017**, *12*, 233–243. [[CrossRef](#)]
 36. Goodger, E.M. *Principles of Spaceflight Propulsion*, 1st ed.; Pergamon Press: Oxford, UK, 1970; p. 15.

Disclaimer/Publisher's Note: The statements, opinions and data contained in all publications are solely those of the individual author(s) and contributor(s) and not of MDPI and/or the editor(s). MDPI and/or the editor(s) disclaim responsibility for any injury to people or property resulting from any ideas, methods, instructions or products referred to in the content.